Langmuir
Article
pubs.acs.org/Langmuir

Thermally Responsive Fluid Behaviors in Hydrophobic Nanopores

Ling Liu,[†] Jianbing Zhao,[†] Patricia J. Culligan,[†] Yu Qiao,[‡] and Xi Chen*,[†]

[†]*Department of Earth and Environmental Engineering, MC 4711, Columbia University, New York, New York 10027, and* [‡]*Department of Structural Engineering, University of California—San Diego, La Jolla, California 92093-0085*

Received April 28, 2009. Revised Manuscript Received July 10, 2009

A fundamental understanding of the thermal effects on nanofluid behaviors is critical for developing and designing innovative thermally responsive nanodevices. Using molecular dynamics (MD) simulation and experiment, we investigate the temperature-dependent intrusion/adsorption of water molecules into hydrophobic nanopores (carbon nanotubes and nanoporous carbon) and the underlying mechanisms. The critical infiltration pressure is reduced for elevated temperature or increased pore size. The variation of wettability is related to the thermally responsive fluid characteristics, such as the surface tension and contact angle, which arise from the variations of multiple atomic variables including the confined water density, hydrogen bond, and dipole orientation. With thermal perturbation, most of these physical quantities are found to be more significantly influenced in the confined nanoenvironment than in the bulk. By utilizing the prominent thermal effect at the nanoscale, the feasibility and prospective efficiency of employing nanofluidics for energy storage, actuation, and thermal monitoring are discussed.

Introduction

The wettability (which is characterized by the contact angle, α) between most liquids and solids can be varied significantly in response to a temperature variation.[1] Thermal gradient is therefore usually utilized to drive a liquid phase to move with respect to a solid phase, know as the thermocapillary effect, e.g., liquid pumping/evacuation and manipulation in microfluidic channels[2,3] and on flat/patterned surfaces.[1,4]

Considering a nanochannel with the diameter of D immersed in a nonwetting liquid ($\alpha > 90°$), an external pressure is required to force the liquid to infiltrate and eventually fill up the channel. According to the classical Young's equation, the critical pressure is determined by $P_{cr} = -4\gamma \cos\alpha/D$, where γ is the surface tension of the liquid. The applicability of the Young's equation at the nanoscale has been verified in our previous work.[5,6] Since both γ and α are functions of temperature, P_{cr} is also a temperature-dependent quantity. Thus, when an external pressure P is applied, it could be above P_{cr} at one temperature while below P_{cr} at another temperature, making the temperature variation a "switch" that controls the infiltration/defiltration of the liquid or the wetting/dewetting of the channel. Accompanying such a transition, the system volume is variable, and the mechanical work is first stored as interfacial energy during infiltration and released by doing work to the environment during defiltration. The efficiency of such a thermally responsive nanosystem can be amplified by nanoporous materials[7,8] that have ultralarge specific pore surface areas, leading to much larger energy density and/or strain output compared with conventional smart/actuation materials. In order to fulfill the promise of the proposed nanoporous thermal machine, it is of fundamental value to understand the thermally responsive behaviors of nanofluids.

When confined in a nanoenvironment, such as nonpolar carbon nanotubes,[5,9,10] polar zeolite pores,[11−15] and cavities of proteins,[16] the behaviors of fluids are often distinct from their bulk counterparts. In particular, if the diameter of the nanopore is comparable to the molecular size, the infiltrated liquid molecules form a quasi-one-dimensional chain and transport as a single file;[9,17] more complex structures such as the n-gonal ring[18] or the double helical chain[11] may emerge when the pressure is sufficiently high. Inside larger nanopores, a multilayered structure is often formed near the tube surface,[19] associated with the less restrictive confinement, water molecules are usually bonded by more hydrogen bonds,[20] and the dipole orientation is more diverse.[21] Similar to these size-dependent molecular structural features, nanofluid characteristics such as the contact angle,[22,23] the infiltration pressure,[11,12] and the apparent viscosity[24] have also been found to strongly depend on the size of the nanopores.

*Corresponding author. E-mail: xichen@columbia.edu.

(1) Kataoka, D. E.; Troian, S. M. *Nature* **1999**, *402*, 794–797.
(2) Sammarco, T. S.; Burns, M. A. *AIChE J.* **1999**, *45*, 350–366.
(3) Darhuber, A. A.; Valentino, J. P.; Davis, J. M.; Troian, S. M.; Wagner, S. *Appl. Phys. Lett.* **2003**, *82*, 657–659.
(4) Pratap, V.; Moumen, N.; Subramanian, R. S. *Langmuir* **2008**, *24*, 5185–5193.
(5) Liu, L.; Qiao, Y.; Chen, X. *Appl. Phys. Lett.* **2008**, *92*, 101927.
(6) Qiao, Y.; Cao, G.; Chen, X. *J. Am. Chem. Soc.* **2007**, *129*, 2355–2359.
(7) Chen, X.; Surani, F. B.; Kong, X.; Punyamurtula, V. K.; Qiao, Y. *Appl. Phys. Lett.* **2006**, *89*, 241918.
(8) Han, A.; Qiao, Y. *Appl. Phys. Lett.* **2007**, *91*, 173123.
(9) Hummer, G.; Rasaiah, J. C.; Noworyta, J. P. *Nature* **2001**, *414*, 188–190.
(10) Joseph, S.; Aluru, N. R. *Nano Lett.* **2008**, *8*, 452–458.
(11) Qiao, Y.; Liu, L.; Chen, X. *Nano Lett.* **2009**, *9*, 984–988.
(12) Liu, L.; Chen, X.; Lu, W.; Qiao, Y. *Phys. Rev. Lett.* **2009**, *102*, 184501.
(13) Desbiens, N.; Demachy, I.; Fuchs, A. H.; Kirsch-Rodeschini, H.; Soulard, M.; Patarin, J. *Angew. Chem., Int. Ed.* **2005**, *44*, 5310–5313.
(14) Eroshenko, V.; Regis, R. C.; Soulard, M.; Patarin, J. *J. Am. Chem. Soc.* **2001**, *123*, 8129–8130.
(15) Cailliez, F.; Trzpit, M.; Soulard, M.; Demachy, I.; Boutin, A.; Patarin, J.; Fuchs, A. H. *Phys. Chem. Chem. Phys.* **2008**, *10*, 4817–4826.
(16) Yin, H.; Hummer, G.; Rasaiah, J. C. *J. Am. Chem. Soc.* **2007**, *129*, 7369–7377.
(17) Alexiadis, A.; Kassinos, S. *Chem. Rev.* **2008**, *108*, 5014–5034.
(18) Koga, K.; Gao, G. T.; Tanaka, H.; Zeng, X. C. *Nature* **2001**, *412*, 802–805.
(19) Thomas, J. A.; McGaughey, A. J. H. *J. Chem. Phys.* **2008**, *128*, 084715.
(20) Gordillo, M. C.; Marti, J. *Chem. Phys. Lett.* **2000**, *329*, 341–345.
(21) Wang, J.; Zhu, Y.; Zhou, J.; Lu, X. H. *Phys. Chem. Chem. Phys.* **2004**, *6*, 829–835.
(22) Liu, L.; Zhao, J.; Yin, C.; Culligan, P. J.; Chen, X. *Phys. Chem. Chem. Phys.* **2009**, DOI: 10.1039/b905641f.
(23) Werder, T.; Walther, J. H.; Jaffe, R. L.; Halicioglu, T.; Noca, F.; Koumoutsakos, P. *Nano Lett.* **2001**, *1*, 697–702.
(24) Chen, X.; Cao, G.; Han, A.; Punyamurtula, V. K.; Liu, L.; Culligan, P. J.; Kim, T.; Qiao, Y. *Nano Lett.* **2008**, *8*, 2988–2992.

Despite these previous research efforts, the influence of temperature on nanofluid behaviors is less explored, which could impose a severe challenge to the prospective applications of the nanoporous thermal machine.

In this paper, molecular dynamics (MD) simulation is employed to investigate the infiltration of water molecules into a model carbon nanotube with varying size and at different temperatures. The dependency of P_{cr} on temperature and nanochannel size unveiled from the numerical simulation is qualitatively verified via an experiment with nanoporous carbon. The temperature-dependent infiltration behavior is attributed to the interplay of multiple physical quantities, i.e., the contact angle, surface tension, water density, hydrogen bond, and dipole orientation, whose thermal dependencies are systematically quantified. The feasibility and prospective efficiency of employing the thermally responsive nanofluid behaviors for building nanodevices are discussed.

Thermally Responsive Nanofluid Infiltration

We first explore the fundamental thermal effect on nanofluid infiltration characteristics. As a model structure of nanochannel, a flexible carbon nanotube (CNT, illustrated in Figure 1) has one of its openings immersed in a reservoir filled with water molecules. The top and bottom surfaces of the reservoir are bounded by two rigid planes, with the upper one fixed and the lower one movable to mimic a piston. Periodical boundary condition is imposed on the four lateral planes of the computational cell. In MD simulation, the interatomic vdW (van der Waals) interaction is described by the 12−6 Lennard-Jones (LJ) empirical force field, $U(r) = 4\varepsilon[(\sigma/r)^{12} - (\sigma/r)^{6}]$, where r denotes the distance between atoms and ε and σ are energy and length parameters, respectively. The Amber96 LJ parameters[25] are adopted for carbon atoms. The flexibility of CNT is addressed by a Morse bond, a harmonic cosine angle, and a 2-fold torsion potential.[26] Water molecules are modeled by the extended simple point charge potential (SPC/E).[27] The carbon−oxygen LJ parameters are extracted from the experimental low-coverage isotherm data of oxygen adsorption on graphite.[28] By using these molecular models and parameters, the graphene as the raw material for constructing CNTs is ensured to be hydrophobic.[29] A 10 Å cutoff is assumed for the vdW interaction. The Nose/Hoover thermostat[30] with a damping parameter of 0.1 is employed to regulate the temperature at 300 K. Long-range electrostatic interaction is estimated by the Ewald summation technique. The time step in MD simulation is set to be 1 fs.

Four representative CNTs, (10,10), (13,13), (15,15), and (20,20), are considered in our study, whose diameter, D, equals 13.56, 17.63, 20.34, and 27.12 Å, respectively. The ambient temperature, T, is varied and assumed to take four representative values: 300, 320, 340, and 360 K, respectively. For a given temperature, a specific number of water molecules are placed in the reservoir such that the initial pressure is close to the ambient (zero) after equilibrium. Next, the water phase is pressurized by moving the piston upward. In order to rule out possible dynamical effects, we carefully load the system in a stepwise and quasi-static manner. In each step, we move the piston by 0.05 Å, after which the position of the piston is temporarily fixed (until the next loading step) and the system is allowed a sufficiently long time to reach equilibrium (where the temperature distribution is close to uniform). Note that the equilibrium time varies throughout the process, on the order of 1 ns after water intrusion and shorter before. Pressure is evaluated every step from the immediate density of water inside the reservoir. The pressure−density relationship adopted in this study, $P = \rho^{6}(T + T_0) - P_0$, is deduced from the data published by IAPWS,[31] where ρ is the density of water (in the unit of g/cm^3), T denotes the ambient temperature, P_0 equals 378 MPa, and T_0 equals 85 K.

As an illustrative example, Figure 2 plots the number of infiltrated water molecules in response to the applied pressure for a (10,10) armchair nanotube at the temperature of 300 K. It is readily seen that water molecules continuously intrude the nanotube only after the pressure exceeds a critical value of about 153 MPa, and the pressure is essentially invariant during the quasi-static

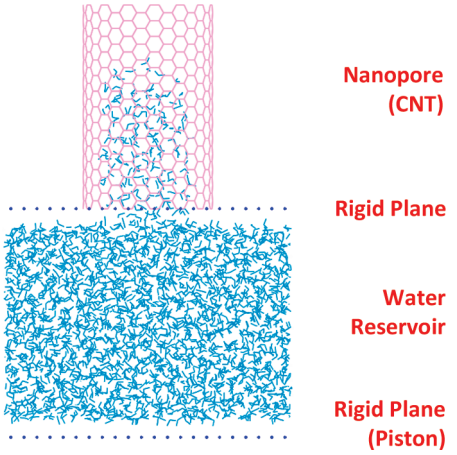

Figure 1. The computational model. One end of a long carbon nanotube (CNT) is immersed in a reservoir filled up with water molecules. The upper rigid plane is fixed while the lower one is movable for adjusting the pressure inside the reservoir. Periodical boundary condition is applied to the four lateral planes of the computational cell.

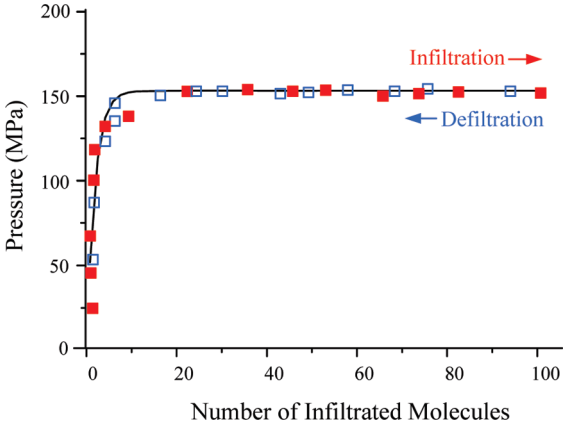

Figure 2. Applied pressure versus the number of infiltrated water molecules in the quasi-static infiltration/defiltration simulation of a (10,10) CNT at the temperature of 300 K. No hysteresis is observed, and a curve is fitted from the data points, which features a plateau at a critical infiltration pressure, P_{cr}.

(25) Cornell, W. D.; Cieplak, P.; Bayly, C. I.; Gould, I. R.; Merz, K. M.; Ferguson, D. M.; Spellmeyer, D. C.; Fox, T.; Caldwell, J. W.; Kollman, P. A. *J. Am. Chem. Soc.* **1995**, *117*, 5179–5197.
(26) Walther, J. H.; Jaffe, R.; Halicioglu, T.; Koumoutsakos, P. *J. Phys. Chem. B* **2001**, *105*, 9980–9987.
(27) Berendsen, H. J. C.; Grigera, J. R.; Straatsma, T. P. *J. Phys. Chem.* **1987**, *91*, 6269–6271.
(28) Bojan, M. J.; Steele, W. A. *Langmuir* **1987**, *3*, 1123–1127.
(29) Werder, T.; Walther, J. H.; Jaffe, R. L.; Halicioglu, T.; Koumoutsakos, P. *J. Phys. Chem. B* **2003**, *107*, 1345–1352.
(30) Hoover, W. G. *Phys. Rev. A* **1985**, *31*, 1695–1697.
(31) Wagner, W.; Pruss, A. *J. Phys. Chem. Ref. Data* **2002**, *31*, 387–535.

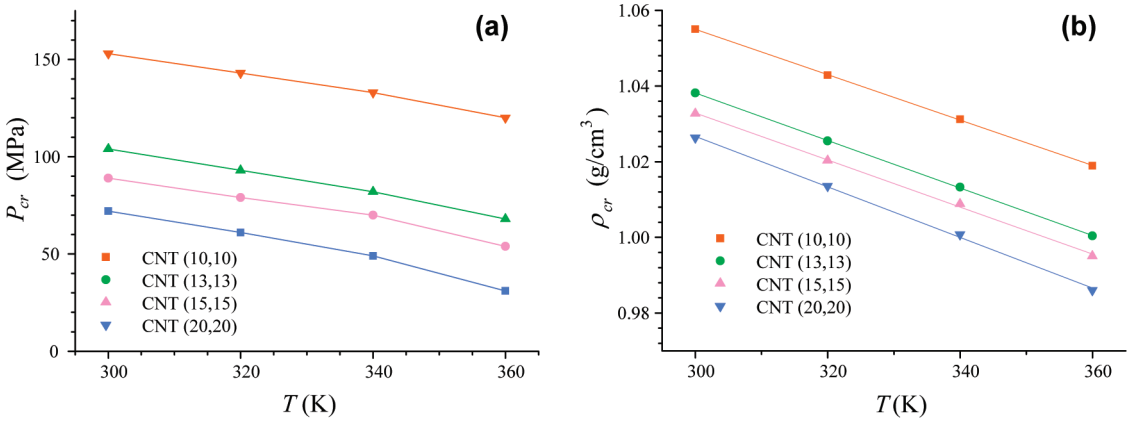

Figure 3. Thermal and size dependencies of the critical infiltration state for carbon nanotubes immersed in water: (a) infiltration pressure, P_{cr}, and (b) water density inside the reservoir, ρ_{cr}. The diameters of CNTs are 13.56, 17.63, 20.34, and 27.12 Å, respectively.

Table 1. Fitting Parameters of the $\rho_{cr}-T$ Relations (Figure 3b) Described by $\rho_{cr} = -kT + \rho'$

CNT	(10,10)	(13,13)	(15,15)	(20,20)
k [10^{-3} g/(cm^3 K)]	0.6687	0.6195	0.6293	0.5998
ρ' [g/cm^3]	1.2272	1.2195	1.2265	1.2350

displacement-controlled infiltration process. Such a critical pressure upon which infiltration occurs, P_{cr}, is also referred to as the infiltration pressure in this paper. Upon unloading, no hysteresis is observed as the loading and unloading paths overlap exactly. This may be attributed to the quasi-statically applied load and the defect-free (nearly frictionless) carbon nanotube. Therefore, in what follows, we focus on the infiltration behavior in this study.

For other nanotubes studied at different temperatures, the overall shape of the continuous water intrusion isotherm is similar to that shown in Figure 2, yet the most critical parameter, P_{cr}, exhibits a strong dependence on the temperature and pore size. As depicted in Figure 3a, for all nanotubes P_{cr} decreases with the increase of temperature, indicating that the energy barrier for water to enter a hydrophobic confined space is effectively reduced at elevated temperatures. If the temperature is fixed, the infiltration pressure is found to vary nonlinearly with the pore size, matching the trend with the Young's equation where P_{cr} is inversely proportional to D. Interestingly, in Figure 3b, the critical density of water, ρ_{cr}, is shown to have an almost linear relationship with the temperature, and the slopes, k, as tabulated in Table 1, are quite close for all CNTs examined. The thermal dependency of P_{cr} is attributable to the interplay of multiple physical quantities, including the contact angle, surface tension, hydrogen bonding, among others, elaborated in the next section.

Underlying Molecular Mechanisms

According to the Young's equation, two quantities are directly related to the thermally responsive infiltration behavior discovered above, namely the contact angle, α, and the surface tension, γ, both of which are important fluid characteristics. In order to quantify their thermal dependencies in the nanoconfinement, a (20,20) CNT is considered as a representative cavity for accommodating water molecules: 1220 water molecules are placed inside the flexible nanotube to form a discrete water drop and simulated for 10 ns at a fixed temperature (without any external load). Molecular trajectories are output every 0.1 ps for statistical purposes. Shown in Figure 4a is the density map for the case with T = 300 K, where it is readily seen that a convex meniscus is formed on top of the liquid drop due to the hydrophobic nature of the considered nanotube. In order to effectively characterize the water front, the spatial positions of boundary water molecules are averaged over all recorded time frames (squared symbols in Figure 4a), which are further fitted by a circular arc-shaped curve leading to the averaged water front (the black curve). α is subsequently deduced as the angle of the tangent of the water front where it meets the lateral surface of the water drop. Further, with the measured α and P_{cr}, γ is calculated according to the Young's equation for the present tube and the temperature.

As plotted in Figure 4b,c, both α and γ are found to decrease at elevated temperatures,[42] and according to Young's equation, both terms contribute to the reduction of P_{cr} with respect to the increasing temperature. The descending trend discovered for α agrees well with the result for a water droplet resting on a graphene.[32] The result for γ qualitatively matches the temperature-induced variation of the surface tension of bulk water in contact with air, γ_{bulk}.[33] Importantly, in Figure 4c γ shows a faster decreasing trend than γ_{bulk}, suggesting that the surface tension is more sensitive to thermal perturbation when confined in a nanoenvironment.

From an atomistic perspective, the uncovered thermal dependencies of surface tension and contact angle are underpinned by the thermally induced variations of multiple quantities. First, hydrogen bonding as an attractive interaction between water molecules is critical to determining water properties such as boiling and surface tension. Two water molecules are considered hydrogen bonded if (1) the O−O distance is below 3.5 Å and (2) the angle between the O−O axis and a O−H bond is smaller than 30°.[34] The averaged number of hydrogen bond per molecule, N_{HB}, may serve as a numerical indicator of the hydrogen bonding. Besides N_{HB}, two other parameters are associated with the strength of the hydrogen bond and thus effectively depict the interaction among water molecules: (1) water density, ρ, which is an indication of the averaged intermolecular distance, and (2) dipole orientation, θ, which quantifies the orientation of the dipole moment with respect to the tube axis. The thermal dependencies of these three quantities are pursued via MD simulations, for a water drop confined in various nanotubes and at various temperatures, elaborated below.

Figure 5 plots the radial distributions of N_{HB} (the dashed curve) and ρ/ρ^* (the solid curve, where ρ is normalized by ρ^*, the bulk water density). Compared with their counterparts in the

(32) Zangi, R.; Berne, B. J. *J. Phys. Chem. B* **2008**, *112*, 8634–8644.
(33) Weast, R. C. *Handbook of Chemistry and Physics*, 61st ed.; CRC Press: Boca Raton, FL, 1981.
(34) Luzar, A.; Chandler, D. *Nature* **1996**, *379*, 55–57.

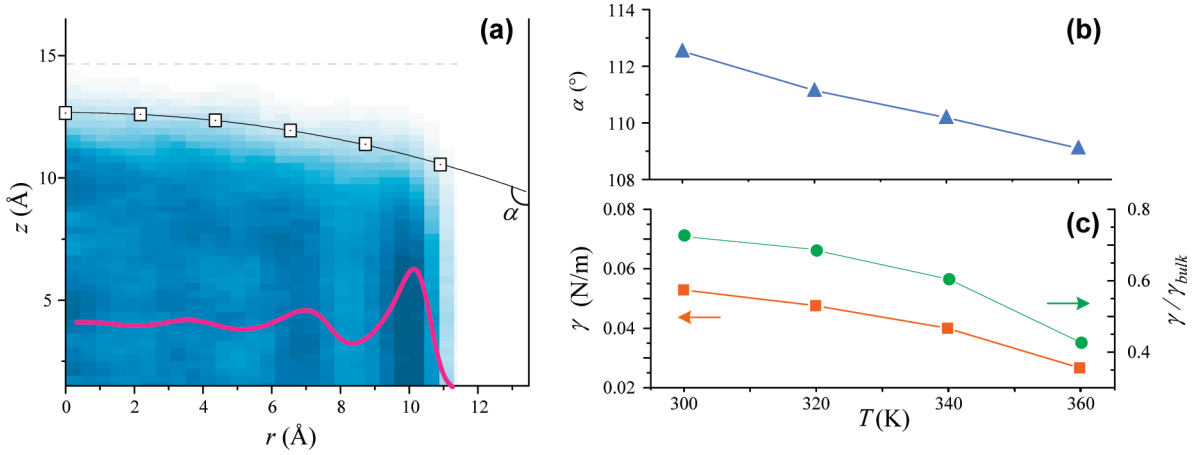

Figure 4. Water confined in a (20,20) carbon nanotube. (a) Density map where the darker color refers to higher density and the lighter color corresponds to lower probability of occupation of water molecules. The left axis overlaps the tube axis, and the right axis indicates the tube surface. The black line fitted from the open squared symbols depicts the statistically averaged water front, based on which the contact angle is determined. The red curve represents the radial density distribution of water molecules (far away from the meniscus), and the variation is consistent with the color gradient in the density map. (b) Evolution of the contact angle, α, with varying temperature. (c) Evolutions of the surface tension γ and the ratio γ/γ_{bulk} with changing temperature.

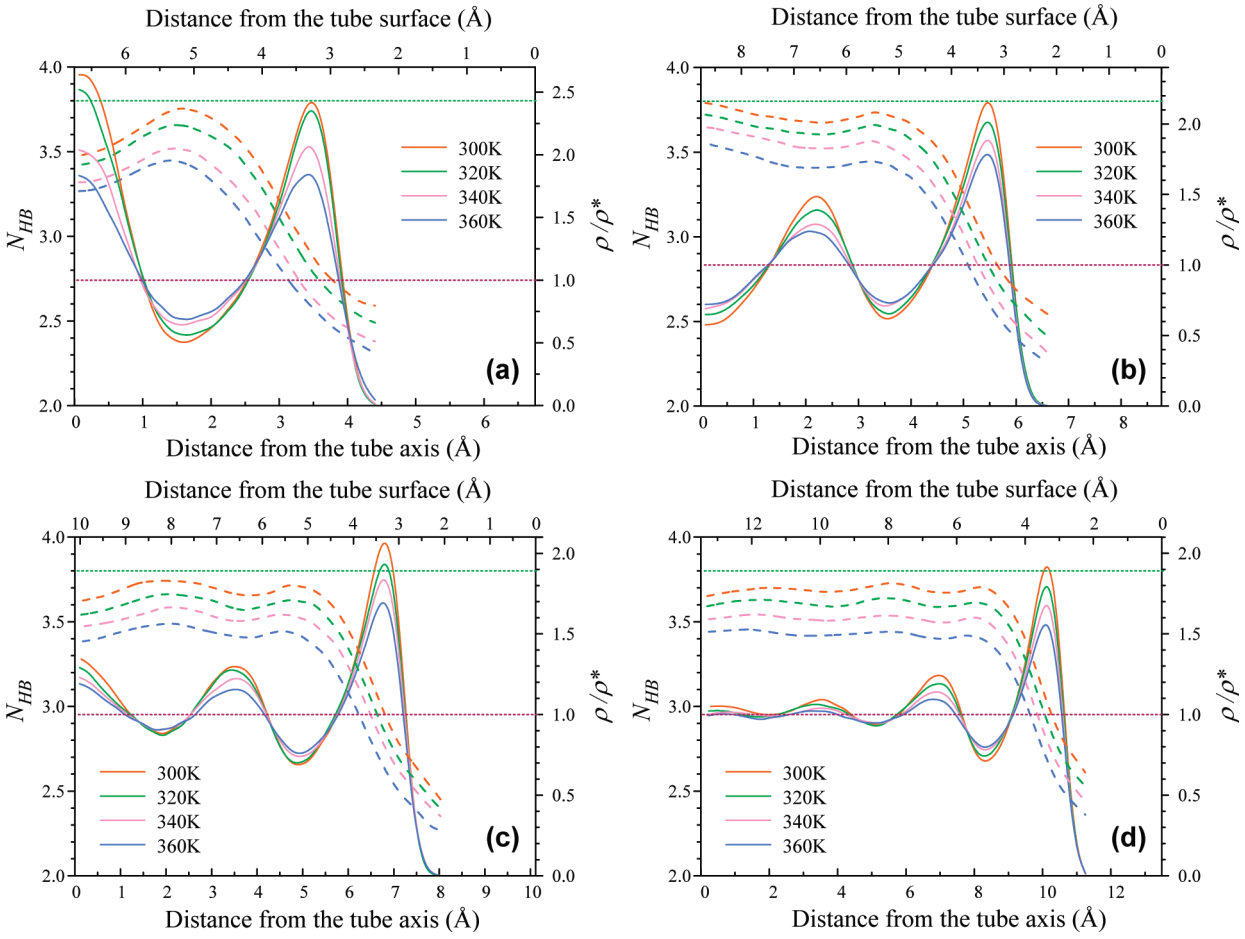

Figure 5. Radial distributions of the averaged number of hydrogen bond per molecule, N_{HB} (the dashed curve), and the normalized water density, ρ/ρ^* (the solid curve), at four representative temperatures for (a) (10,10) CNT, (b) (13,13) CNT, (c) (15,15) CNT, and (d) (20,20) CNT. In each figure, the left axis overlaps the tube axis and the right axis indicates the tube surface. Two reference horizontal lines are shown: the purple one refers to the bulk water density ($\rho/\rho^*=1.0$), and the green one corresponds to the value of N_{HB} measured in bulk water at room temperature (~3.81).

bulk phase, N_{HB} in the confined water is always smaller, whereas ρ moderately fluctuates about ρ^*. Interestingly, the fluctuations of N_{HB} and ρ conform to opposite trends; that is, a crest of N_{HB} often corresponds to a trough of ρ and vice versa. This implies that a higher concentration of water molecules may to some extent distort the angle between the O−O axis and the

O−H bond, leading to less probability of forming hydrogen bonds.

With the temperature increased from 300 to 360 K, N_{HB} decreases almost linearly at all radial positions, whereas ρ decreases in crests and increases in troughs (and thus its fluctuation is reduced). Very importantly, the thermal effect is found to be more significant in the confined water than in the bulk. For instance, from 300 to 360 K, the density of water in the (20,20) CNT is reduced by 21% at the outmost peak and increased by 14% at the second peak; by contrast, the density of bulk water only shows a 2.9% reduction in response to the same thermal perturbation. Another example is the thermally induced (for temperature increased from 300 to 360 K) variation of the line number density of water molecules (the number of water molecules confined in a nanotube of unit length), $\overline{N}$, which according to Table 2 is estimated as 11.4%, 8.7%, 7.8%, and 7.4% for CNTs of increasing sizes. This further verifies that the thermal effect is more prominent in a narrower nanoconfinement. The stronger thermal effect in the confined water indicates that fluid properties should be more sensitive to thermal factors in nanoconfinement than in the bulk, which echoes our findings about the surface tension in Figure 4b.

Table 2. Line Number Density, $\overline{N}$, of Water Molecules Confined in Carbon Nanotubes [1/Å]

CNT	(10,10)	(13,13)	(15,15)	(20,20)
300 K	2.4194	4.8246	6.9218	13.9458
320 K	2.3417	4.7126	6.7595	13.6293
340 K	2.2147	4.5374	6.6256	13.2642
360 K	2.1448	4.4065	6.3836	12.9141

With reference to the multilayered density distribution of water molecules inside the CNT, Figure 6 plots the probability of θ for two groups of water molecules separately. One group (the dashed curve) refers to the outmost layer of the water column, and the other (the solid curve) includes all of the rest water molecules. The two groups of water molecules exhibit distinct dipole orientations. In the outmost layer, primarily due to the direct and strong interaction with solid atoms, water molecules are more uniformly orientated than the inner molecules and show a strong tendency to align with the tube axis. As a result, the probability of forming hydrogen bonds is effectively lowered, which is readily reflected in Figure 5 where N_{HB} decays quickly in the region of the outmost layer. Figure 6 also shows that the dipole orientation is much less sensitive to the thermal variation than other quantities investigated in this paper, implying less contribution from θ to the apparent thermally responsive nanofluid behaviors.

Experimental Verification and Prospects of Thermally Responsive Nanofluids

In order to verify the discovered thermal effect on the infiltration pressure, an infiltration experiment with a Norix nanoporous carbon was performed. The as-received material was in the form of 50−100 μm powders. About 2 g of the material was placed in a steel mold and compressed in a type 5580 Instron machine at either 0.5 MPa (sample A) or 15 MPa (sample B), forming densely packed powder cluster disks. The disks were milled back to the powder form, and the nanoporous structure was characterized by a Micromeritics ASAP-2000 gas absorption analyzer. The average nanopore size of sample A was 50 Å, and that of sample B was 30 Å. The specific surface areas of both samples were around 550 m^2/g.

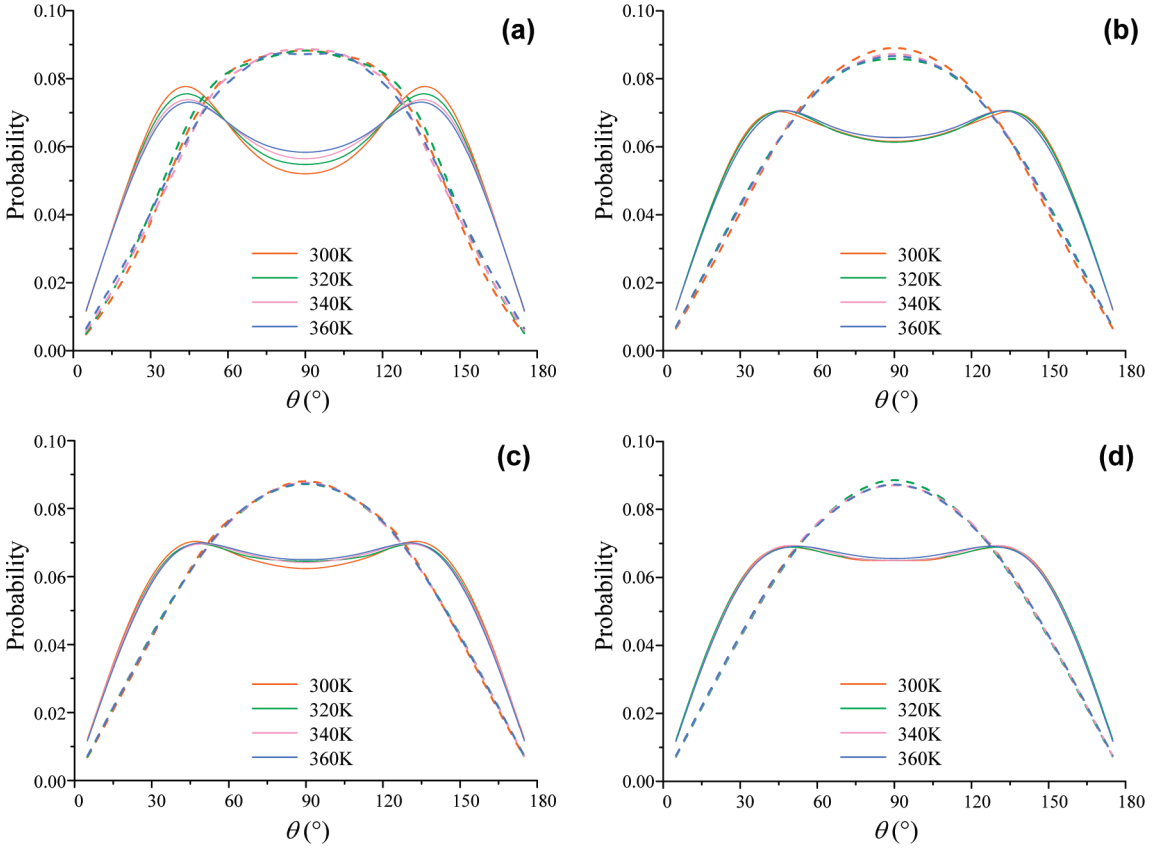

Figure 6. Probability of dipole orientation with respect to the tube axis, θ, at four representative temperatures for (a) (10,10) CNT, (b) (13,13) CNT, (c) (15,15) CNT, and (d) (20,20) CNT. Two groups of water molecules are analyzed separately: one group (the dashed curve) refers to the outmost layer in the multilayered water structure (the first wave to the right axis in the density profile, Figure 5), which is usually the most concentrated region, and the other (the solid curve) includes all of the rest of the water molecules.

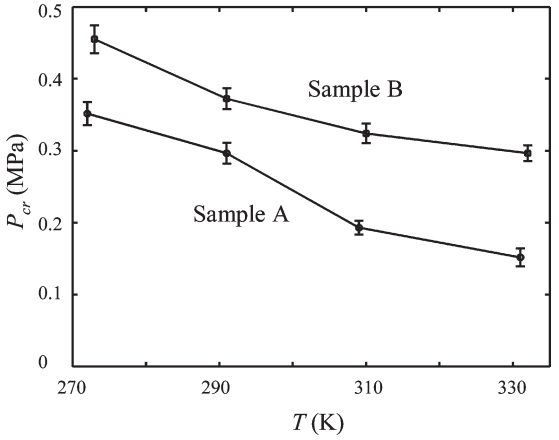

Figure 7. Measurement results of infiltration pressure for nanoporous carbon immersed in water. The average nanopore size of sample A is 50 Å, and that of sample B is 30 Å.

About 0.25 g of the treated material (the detailed surface treatment process was described elsewhere[35]) was sealed in a steel cylinder with 6 g of deionized water. By using the Instron machine, a steel piston was intruded in the cylinder at a speed of 1 mm/min (the loading rate was confirmed to be sufficiently slow so as not to introduce any rate effect). The diameter of the piston was 19 mm. Because the nanopore inner surfaces were hydrophobic, only when the applied pressure was sufficiently high (beyond P_{cr}) could a large number of water molecules be forced into the nanopores. The medium pressure associated with the pressure induced infiltration was measured by a 2 kN load cell. During the testing process, the temperature of the sample was maintained by a water bath around 270, 290, 310, or 330 K.

The measured results are plotted in Figure 7, which qualitatively agree with the computational results shown in Figure 3a, both suggesting decreasing P_{cr} with increasing T or D. Note that the experimental measurements might be affected by surface treatment[35,36] and nonuniform pore size,[37] among others, which effectively lowered the infiltration pressure and led to the data scattering in the $P_{cr}-T$ curves.[43] Nevertheless, the trend of the variation of infiltration is qualitatively consistent between the experiment and simulation, and experiments with better controlled surface structure/treatment and pore size will be carried out in the future.

A word of caution is that our finding of the temperature effect may not be extrapolated to extremely small nanopores, e.g., silicalite-1 zeolite with the diameter of about 5.4 Å.[15] Inside such a small nanopore whose cross section may accommodate only one water molecule, the invaded water molecules are expected to have molecular behaviors (e.g., hydrogen bonding,[9] dipole orientation,[21] and thermal vibration characteristics) very different from those confined in larger pores. Furthermore, under this circumstance the polarization of nanopores must play an important role on the infiltration/transport behaviors of confined liquids.[38] The detailed temperature effect on water infiltration into very small nanopores will be carried out in the future.

As noted in the Introduction, a thermally responsive nanosystem is enabled by the thermal switching between wetting and dewetting of the extremely fine pores of nanoporous materials. According to a Carnot cycle analysis,[39] the net output energy is approximated by $P\Delta V$, where P is the working pressure and ΔV is the pore volume density. For sample B of nanoporous carbon, the energy density is estimated as 0.4 J/g, much larger than that of Ti−Ni alloys, 50 mJ/g. The output energy density of the nanoporous system may be further enhanced by enhancing either the working pressure or the pore volume density. As a perspective example, based on the simulation results of the (13,13) CNT where the pore volume density is about 0.3 cm^3/g, a working pressure of 100 MPa (which is below P_{cr} at 300 K but exceeds the threshold at 310 K, according to Figure 3a) can, theoretically, yield a considerably high output mechanical energy at the level of 10 J/g.

Besides the above potential as a nanoporous thermal machine working under a constant pressure, the linear $\rho_{cr}-T$ relationship revealed in simulation provides an alternative route to building nanothermometers.[40] Inside a partially wetted nanotube immersed in a volume-fixed reservoir (at an appropriate pressure level), the advancement and recession of the water front are linearly related to the temperature variation, as described by $\Delta h = k\Delta T V_r/m_0\bar{N}$, where Δh is the height variation of the confined water in the nanotube, ΔT the temperature change, V_r the volume of the reservoir, k the slope of the $\rho_{cr}-T$ relation as tabulated in Table 1, m_0 the density of a water molecule, and $\bar{N}$ the line number density of confined water molecules as tabulated in Table 2. Apparently, with a sufficiently large reservoir (large V_r) and a small nanopore (low $\bar{N}$), a considerably high sensitivity ($\Delta h/\Delta T$) may be achieved, making the proposed nanothermometer superior to those purely based on the thermal expansion mechanism.[41]

Concluding Remarks

This paper investigates the fundamental thermal effect on the infiltration of water molecules into hydrophobic nanopores. Both MD simulation (on CNT) and experiment (on nanoporous carbon) confirm that the critical infiltration pressure increases with either lowered temperature or reduced pore size. The reduced hydrophobicity at elevated temperature is underpinned by the thermally induced variations of multiple quantities, such as surface tension, contact angle, hydrogen bond, intermolecular distance, and dipole orientation. The thermal dependencies of these parameters are systematically quantified via MD simulations. A general finding is that the thermal effects on these atomic/fluid variables are more significant in a confined nanoenvironment than in the bulk. Increasing the temperature can reduce the contact angle, surface tension, hydrogen bond number density, and water line number density and make the water radial density distribution less fluctuating.

The more prominent thermal effects at the nanoscale are expected to enable high efficiency of thermal nanodevices. For example, on the basis of thermally controlled switching of wetting/dewetting of nanopores, a nanoporous thermal machine is proposed, which is estimated to store and output more energy per mass than conventional materials. Moreover, since the critical water density inside the reservoir varies linearly with temperature, a nanothermometer is proposed which features competitive sensitivity to the thermal perturbation. Although the findings of this paper are extracted from the model system of the infiltration

(35) Han, A. J.; Qiao, Y. *Chem. Lett*. **2007**, *36*, 882–883.
(36) Han, A.; Punyamurtula, V. K.; Qiao, Y. *Chem. Eng. J*. **2008**, *139*, 426–429.
(37) Han, A.; Lu, W.; Punyamurtula, V. K.; Chen, X.; Surani, F. B.; Kim, T.; Qiao, Y. *J. Appl. Phys*. **2008**, *104*, 124908.
(38) Won, C. Y.; Joseph, S.; Aluru, N. R. *J. Chem. Phys*. **2006**, *125*, 114701.
(39) Soulard, M.; Patarin, J.; Eroshenko, V.; Regis, R. E.; van Steen, M. C.; Callanan, L. H. In *Studies in Surface Science and Catalysis*; Elsevier: Amsterdam, 2004; Vol. *154*, Part 2, pp 1830−1837.
(40) Lee, J.; Kotov, N. A. *Nano Today* **2007**, *2*, 48–51.
(41) Gao, Y. H.; Bando, Y. *Nature* **2002**, *415*, 599–599.
(42) Although Figure 4 is specified for a (20,20) tube, the same trend of thermal effect is observed for CNTs of different sizes. The size dependency of the contact angle has been studied in the literature,[19,20] and we focus on thermal effects in this study.
(43) Detailed investigation of the effects of surface treatment and pore size are beyond the scope of the current paper, which focuses on the temperature effect.

of water molecules into carbon nanotubes, the overall thermal effect is expected to be prominent for other nanofluid phases confined in different nanochannels. For different combinations of fluids/nanochannels, the different details of the thermal effect are envisioned to enrich the relevant applications of thermally responsive nanofluidic devices.

Acknowledgment. The work was supported by the NSF and the Sandia National Lab under Grant CMMI-0623973 (Y.Q) and the NSF under Grant CMMI-0643726 (X.C). L.L. acknowledges the support of the Founder's Prize, through the American Academy of Mechanics, sponsored by the Robert M. and Mary Haythornthwaite Foundation.